Far-Ultraviolet Imaging Spectroscopy of Io's Atmosphere with HST/STIS

F. L. Roesler, H. W. Moos, R. J. Oliversen, R. C. Woodward Jr.,* K. D. Retherford, F. Scherb, M. A. McGrath, W. H. Smyth, P. D. Feldman, D. F. Strobel

Well-resolved far-ultraviolet spectroscopic images of O I, S I, and previously undetected H I Lyman-α emission from Io were obtained with the Hubble space telescope imaging spectrograph (STIS). Detected O I and S I lines (1250 to 1500 angstroms) have bright equatorial spots (up to 2.5 kilorayleighs) that shift position with jovian magnetic field orientation; limb glow that is brighter on the hemisphere facing the jovian magnetic equator; and faint diffuse emission extending to ~20 Io radii. All O I and S I features brightened by ~50 percent in the last two images, concurrently with a ground-based observation of increased iogenic [O I] 6300-angstrom emission. The H I Lyman-α emission, consisting of a small, ~2-kilorayleigh patch near each pole, has a different morphology and time variation.

Jupiter's strong magnetic field and volcanism on Io, the closest of the Galilean satellites, combine to create dynamic physical features in the jovian system, including the Io plasma torus: a plasma predominately of O and S surrounding and corotating with Jupiter near Io's orbit. Detailed and accurate information on Io's extended atmosphere and neutral clouds is vital for understanding the satellite's interaction with the plasma torus and the jovian magnetosphere, but observations of these neutral gases—including the atomic O and S that feed the torus—have proven challenging. Near Io, visible-light observations must contend with the reflected solar continuum (*1*) or be taken during an eclipse of Io (*2*). More than a few Io radii (R_{Io}) from Io the visible emission lines, with the important exceptions of the minor components Na I and K I, are faint. Several researchers have observed Io and its environs in the bright ultraviolet (UV) emission lines of O I and S I (*3–7*); none of the available UV instruments, however, had sufficient resolution to study the spatial structure of these emissions in detail until the STIS (*8*, *9*) was installed on the Hubble space telescope (HST) in February 1997. We report here observations of Io made with the STIS to try to detect features in Io's atmosphere and exosphere related to its interaction with the jovian magnetosphere and plasma torus.

Observations. The observations consist of two "visits" of Io of three orbits each on 26 September and 14 October 1997 near western (receding) elongation. ("Orbit" refers to an HST orbit in this work, unless otherwise specified.) During each orbit, two spectrally resolved images were acquired in "time-tag" mode (*10*), yielding, after processing with the standard STIS "pipeline" software (*11*), 12 1024 pixel by 1024 pixel images. We used a 52 arc sec by 2 arc sec slit: wide enough to include the disk of Io (1.15 arc sec or 37 pixels in September, and 1.10 arc sec or 45 pixels in October) and its immediate surroundings in the direction of dispersion, and long enough to capture features 15 to 20 R_{Io} away in the spatial direction (*12*). The data therefore show distinct images of Io at each emission line or multiplet, with a separation distance determined by the grating's dispersion. To balance wavelength coverage and spectral resolution, we used three different gratings (*8*) during the experiment: the medium-resolution G230M (*13*) and G140M gratings in September, tilted to observe the S I] λ1900 (wavelength 1900 Å semiforbidden neutral S) multiplet and the O I] λ1356 and S I λ1389 multiplets, respectively; and the low-resolution G140L grating in October, to observe several O I and S I multiplets simultaneously (at the expense of blending multiplet components). The observational parameters are listed in Table 1. The distinct images of Io in different emission wavelengths give the raw data the appearance of a multiple exposure (Fig. 1). The Io plasma torus emission, terrestrial airglow, and instrumental artifacts are also present in the images.

Oxygen and sulfur. The medium-resolution observations 3a and 3b (Table 1) in September detected the O I] λ1356 and S I λ1389

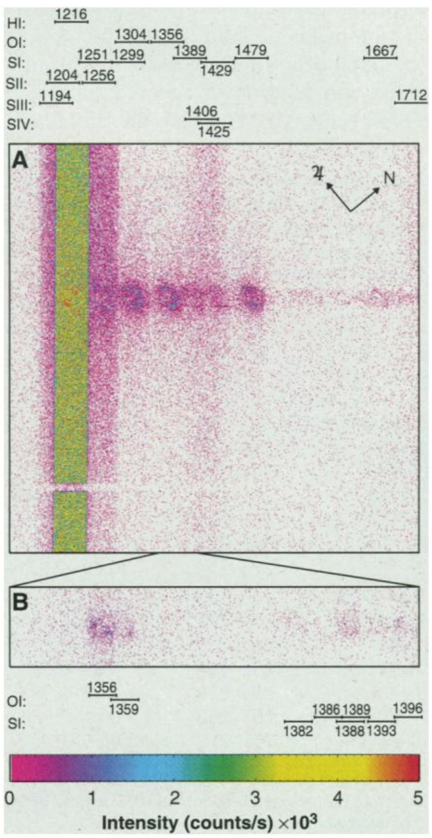

Fig. 1. (**A**) Sum of raw data from the second images of orbits 4 to 6: 1024 pixels by 1024 pixels 0.0244 arc sec squared spatially, with 0.584 Å/pixel dispersion convolved with the spatial information horizontally. The circular features in a row just above mid-image are images of iogenic emission at various O I and S I multiplets; faint, diffuse emission extends above and below the brighter circular features. The vertical green bar is an image of the 52–arc sec by 2–arc sec slit filled with diffuse terrestrial H I Lyman-α emission. Two patches of iogenic H I Lyman-α emission can be seen in the midst of this terrestrial airglow. Also present are several plasma torus lines (vertical bars brighter at the top than the bottom) and the shadow of a 0.5–arc sec fiducial bar in the slit (horizontal band near the bottom). The key above shows the slit positions for various emission wavelengths. The compass shows the directions of Jupiter (east) and jovian north. (**B**) Band from sum of raw data from both images of orbit 3: 1024 pixels by 200 pixels encompassing Io and vicinity. The slit is the same as in (A), but the spatial scale is slightly different (0.031 arc sec/pixel by 0.029 arc sec/pixel), and the spectral resolution is 0.053 Å/pixel. The multiplet components of O I] λ1356 and S I λ1389, as indicated in the key below, are evident; not shown is faint extended emission similar to that in (A). Connecting lines show where the spectral range of (B) maps to (A) at mid-slit.

F. L. Roesler, R. C. Woodward Jr., and F. Scherb are in the Physics Department, University of Wisconsin, 1150 University Avenue, Madison, WI 53706, USA. H. W. Moos, K. D. Retherford, and P. D. Feldman are in the Department of Physics and Astronomy, Johns Hopkins University, Baltimore, MD 21218, USA. R. J. Oliversen is in the Laboratory for Astronomy and Solar Physics, NASA–Goddard Space Flight Center, Greenbelt, MD 20771, USA. M. A. McGrath is at the Space Telescope Science Institute, Baltimore, MD 21218, USA. W. H. Smyth is with Atmospheric and Environmental Research, Cambridge, MA 02139, USA. D. F. Strobel is in the Department of Earth and Planetary Science, Johns Hopkins University, Baltimore, MD 21218, USA.

*To whom correspondence should be addressed.

multiplets; fluxes were calculated for the brighter components of these multiplets (Table 2). The low-resolution observations in October detected O I] λ1356, S I λλ1389, 1429, 1479, 1667, and a blend of O I λ1304 and S I λ1299 (*14*); fluxes were calculated for the brighter of these multiplets (Table 3). These fluxes are consistent with earlier work (*3*, *5*). Morphologically, each image of each line or multiplet is similar: two bright spots above Io's limb near its equator (which we call "equatorial spots"); diskwide emission enhanced along the limb at all Iocentric latitudes ("limb glow"); and fainter emission more than 1 R_{Io} beyond Io's disk, dropping rapidly in intensity with distance from Io ("extended emission"). The extended emission can be seen in Fig. 1, most notably in the O I] λ1356 and S I] λ1479 multiplets; the near-Io emission at selected times and wavelengths is shown in detail in Fig. 2.

Equatorial spots. Enhanced emissions near Io's equator were seen in broadband visible and near-infrared (NIR) images from Galileo's solid state imaging (SSI) experiment (*15*) and [O I] λ6300 images from the HST wide-field planetary camera (WFPC2) (*2*), and inferred from rastered sets of scans of iogenic UV emission from the HST's faint object spectrograph (FOS) (*4*, *16*) and Goddard high-resolution spectrograph (GHRS) (*4*, *17*), but the STIS data show equatorial spots of UV O I and S I emissions in unprecedented detail. The spots are brightest [up to 2.5 kilorayleighs (*18*)] at ~ 200 km above Io's surface and extend several hundred kilometers above that height. At Io's central meridian, emission intensities near the equator are less than or equal to those at higher and lower latitudes; therefore, these equatorial spots on Io's limb are unlikely to be a viewing-geometrcal enhancement of an equatorial ring of emission. The sub- and anti-jovian positions of the spots suggest that they are associated with the Birkeland currents that flow through Io or its ionosphere (*19*). The western, anti-jovian spot has a consistently greater flux and is usually brighter than the eastern, sub-jovian spot. [Viewing geometry may be partially responsible for the observed asymmetry in the first and second HST orbits (Fig. 2, A and C), but not the third (Fig. 2, B and D), of each visit.] This flux asymmetry could be a consequence of asymmetry in the directions of the electron and ion convection patterns as a result of anisotropic ionospheric Hall conductivity (*20*), of a greater abundance of gases from local volcanos, or of a higher SO_2 column density that is expected on the more recently sunlit hemisphere of Io. Observations at eastern elongation could distinguish the last possibility from the first two. Additionally, the spots change Iocentric latitude as Io's jovian magnetic latitude changes (Fig. 2, A to D). This is consistent with an association of the spots with the Birkeland currents; the tangent points of the magnetic field lines at Io would, as a result of the motion of the tilted jovian magnetic field past Io, rotate or rock about Io's equator (Fig. 3). The spots tilt in the same sense as the dipole tangent points, but not always by the same amount. This is not surprising, because the magnetic field near Io is known to be distorted by Birkeland currents, nearby plasma currents, and possibly an intrinsic Ionian field (*21*). In contrast, visible and NIR Galileo SSI images taken over 14 eclipses of Io show sub- and anti-jovian glows that do not change position with magnetic latitude (*22*), but appear to be fixed near known centers of volcanic activity and a newly discovered subjovian field of vents (*23*). Because the SSI filters have broad passbands, however, it is not clear what causes these glows. One way to reconcile our results with those of Galileo is to postulate that Io's volcanos produce relatively immobile local concentrations of gases that are imaged by SSI, and that Birkeland currents excite (and perhaps produce) atomic O and S at varying positions within these gas concentrations.

Limb glow and extended emission. The less intense limb glow lies on or barely above (≲100 km) Io's limb. It is presumably a limb brightening of an all-disk glow and may indicate the presence of a global or hemispherical atmosphere containing S and O. Comparison of orbit 3, when Io was north of the centrifugal equator (*24*) (Fig. 2B), and orbits 4 to 6, when it was south (Fig. 2, C and D), show that the limb glow is consistently brighter on the side facing the equator (Table 1). Similar results have been found in images of [O I] λ6300 emission (*2*). Because Io's diameter (3630 km) is small compared with the latitudinal scale height of the Io plasma torus (~10^5 km), and the bulk torus electron density changes less than 0.1% across Io (*25*), we would not expect this asymmetry in the limb glow to be related to the torus. However, modeling (*20*) and observations by Galileo (*26*, *27*) indicate that plasma near Io slows to 1 to 2 km/s; therefore, >97% of the total electrons in a flux tube could potentially reach Io's atmosphere while the flux tube intersects Io. The greater electron column density above the hemisphere facing the centrifugal equator could thus be responsible for the enhanced emission.

Spatially extended emission in O I λλ1304, 1356, and S I λ1479 is detectable along the slit out to ~20 R_{Io}; it can be seen directly in the raw data (Fig. 1) as faint vertical bands tapering off away from Io and is plotted (for S I λ1479, orbits 4 to 6) in Fig. 4. It drops off approximately as $1/r$ (r is the distance along the slit from the center of Io's disk in the image), the expected behavior for a simple spherically symmetric outflow of gas.

Intensity variations with time. During orbit 6, the O I and S I emission features increased in intensity by a factor of ~1.5 when compared with the previous two orbits that night (Table 3), as well as when compared with the final orbit on 26 September (Table 2). This bright-

Table 1. Instrumental and Iocentric parameters. Io's rotational period is tidally locked to its orbital period, with 0° longitude defined as the average longitude of the sub-jovian spot; thus, Io's central meridian longitude (CML) is equivalent to its orbital phase, with 0° occurring when Io is farthest from the observer. System III is the jovian magnetic longitude system. z_c is the distance of Io north (N) or south (S) of the centrifugal equator (*24*), calculated for an offset tilted dipole magnetic field, in units of the jovian equatorial radius (71,400 km).

Orbit no.*	Starting time (UT)	Integration time (s)	Io system III longitude (°)	Io CML (°)	z_c (R_J)
		26 September 1997 (data set O49D02)†			
1a	10:29	900	79–86	242–244	0.36–0.29 S
1b	10:48		87–94	245–247	0.28–0.20 S
2a	11:51	1180	117–126	253–256	0.05–0.16 N
2b	12:18		129–138	257–260	0.19–0.29 N
3a	13:34	1100	164–173	268–271	0.53–0.58 N
3b	13:56		175–183	271–274	0.59–0.63 N
		14 October 1997 (data set O49D01)‡			
4a	2:45	920	349–356	240–242	0.55–0.59 S
4b	3:04		357–4	243–245	0.59–0.62 S
5a	4:07	1180	27–36	252–254	0.65–0.63 S
5b	4:34		39–48	255–258	0.62–0.58 S
6a	5:44		71–80	265–268	0.41–0.32 S
6b	6:11		84–93	269–272	0.29–0.19 S

*Orbits 1 and 2: wavelength range 1888 to 1978 Å, dispersion 0.087 Å/pixel; orbit 3, 1344 to 1398 Å, 0.053 Å/pixel; orbits 4 to 6, 1150 to 1730 Å, 0.584 Å/pixel. †Pixel size: 0.031 arc sec (dispersion direction) by 0.029 arc sec, or 96 km by 91 km at Io. ‡Pixel size: 0.024 arc sec squared, or 81 km squared at Io.

Table 2. Fluxes of O and S lines observed during orbit 3 (26 September), integrated over a 2 arc sec by 4 arc sec box centered on Io.

Species	Wavelength (Å)	Flux (10^3 photons cm^{-2} s^{-1})
O I	1355.60	1.46 ± 0.15
	1358.52	0.45 ± 0.15
S I	1388.43	0.39 ± 0.17
	1396.11	0.28 ± 0.16

ening (Fig. 5) occurred in all O and S multiplets and in all morphological features of each multiplet image (compare Fig. 2D with Fig. 2, B and C). We obtained simultaneous spectra of [O I] λ6300 emission from Io at Kitt Peak before, during, and after the October orbits (*28*). These data show that iogenic [O I] λ6300 emission increased in intensity simultaneously with the UV multiplets, but by a factor of about 3.5 (Fig. 5), and therefore that the ratios of the UV multiplets to the visible line decrease by about 60%. Our earlier [O I] λ6300 data (*1*) indicate that such large increases in intensity are uncommon, but not unprecedented. Although this brightening coincides with Io's approach to the centrifugal equator, the ground-based data show a sharp drop in emission intensity shortly after the end of the final orbit—just as Io crosses the centrifugal equator, where electron density is expected to be highest. Moreover, the [O I] λ6300 (*29*) and UV emissions (*17*) have exhibited frequent, more modest fluctuations in intensity, on the scale of 15 min or less. The simultaneous brightening of all spatial features of O and S in the STIS images seems inconsistent with sudden outbursts of gas from volcanic vents or other neutral cloud inhomogeneities as explanations. We suggest that large-scale local variations in plasma properties might be responsible; an increase in electron density and decrease in temperature, for example, would be consistent both with the increase in the absolute intensities of the UV and visible emissions and with the decrease in their ratio.

Lyman-α. The most surprising result is the unexpected observation of H I Lyman-α emission near the poles of Io. Lyman-α near Io was initially reported in Pioneer 10 UV photometer data (*30*), but was later discarded after the identification of bright O and S lines within the photometer's passband of 200 to 1400 Å (*31*). In earlier UV spectra of Io, acquired from Earth orbit with the HST/FOS (*5*), HST/GHRS (*4*), Hopkins ultraviolet telescope (HUT) (*6*), and international ultraviolet explorer (IUE) (*3*), the strong terrestrial H I Lyman-α airglow obscured any emission from Io that might have been present, but the imaging capability of the STIS makes it straightforward to distinguish the spatially uniform terrestrial emission from localized iogenic H I Lyman-α (*32*). However, H and H-bearing molecules are not thought to be present on Io's surface or in its atmosphere in significant quantities (*33*); we were therefore surprised to find two H I Lyman-α emission features, with $\sim 3 \times 10^{-4}$ photons cm^{-2} s^{-1} total flux and ~2 kilorayleighs peak intensity, in our data (*34*).

The H I Lyman-α emission (Figs. 2E and 6) differs from the O I and S I emissions we observed. Most of it is concentrated in two bright patches near Io's poles rather than near the equator. Although the patches are reminiscent of terrestrial auroras, they are on the opposite sides of the rotational poles from the presumed entry points of the jovian magnetic field lines. There is no overall disk or limb glow, but the photon noise from the terrestrial airglow would prevent the detection of any features much fainter than a kilorayleigh. Also, unlike emission from the heavier neutrals, the H I Lyman-α patches lie almost entirely within Io's disk, suggesting a source on or near Io's surface. The larger and brighter patch is in the southern hemisphere, the hemisphere away from the centrifugal equator. Finally, during the simultaneous brightening of the O I and S I UV multiplets and the [O I] λ6300 emission seen from the ground, neither patch of H I Lyman-α showed significant brightening (Fig. 5).

It is far from obvious how such emission could arise. Iogenic H may be present in polar caps of H-bearing frost. There is some infrared evidence for surface H_2S (a common volcanic gas on Earth) in the polar regions of Io (*35*, *36*), but the high vapor pressure of H_2S implies a polar temperature at the low end of the expected range (*37*). H_2O has a much lower vapor pres-

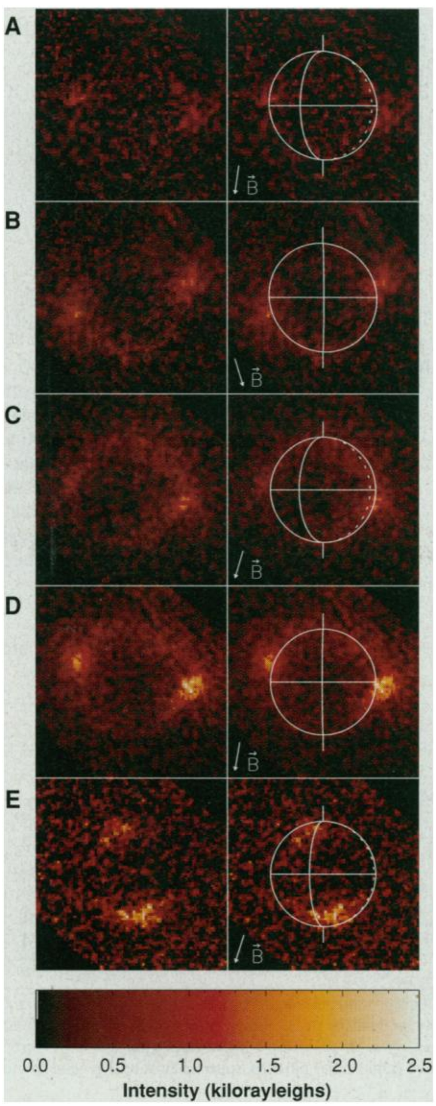

Fig. 2. Details of various emission features near Io. (**A**) S I] λ1900, orbit 1, λ_{III} = 87°; (**B**) O I] λ1356, orbit 3, λ_{III} = 174°; (**C**) O I] λ1356, orbit 4, λ_{III} = 357°; (**D**) O I] λ1356, orbit 6, λ_{III} = 82°; (**E**) H I Lyman-α, orbits 4 to 6. The images have been calibrated and rotated so that Ionian north is up and Jupiter is to the left. The two images from the appropriate orbit have been averaged in rows A to D, and the three images from the second half of each of orbits 4 to 6 have been averaged in row E (to reduce airglow contamination). Each box in the first column is a 2 arc sec by 2 arc sec subimage (65 pixels by 68 pixels for rows A and B; 81 pixels by 81 pixels for rows C to E) centered on Io at a particular wavelength. The second column duplicates the first, with the following features of Io marked: limb (circle), equator (horizontal line), poles (vertical lines), lines of longitude at 180° (dashed half-ellipse) and 270° (solid half-ellipse), and direction of local magnetic field (arrow). (The circles are slightly elliptical in rows A and B to account for the difference in plate scales along and across the direction of dispersion. Because of difficulties in precisely locating Io on the MAMA, we estimate that the positions, but not the scales or orientations, of these diagrams may be off by as much as two pixels.) Note in particular that (i) a line connecting the bright spots is nearly perpendicular to the magnetic field for all O and S images (A to D), but not H (E); (ii) O I] λ1356 is significantly brighter during orbit 6 (D) than orbits 3 and 4 (B and C); (iii) Io's southern limb is brighter than its northern during orbit 3 (B), but its northern limb is brighter during orbits 4 and 6 (C and D); and (iv) the bulk of the O and S emission is on or above the limb (A to D), whereas the H emission is almost entirely within the limb.

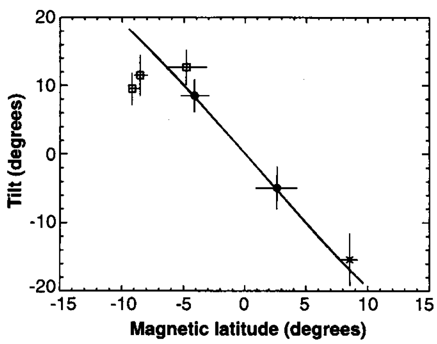

Fig. 3. Plot of tilt (with respect to Ionian equator) of lines connecting centroids of Io's "equatorial spots," in one bright line per orbit, as a function of Io's jovian magnetic latitude at mid-orbit. (●, S I λ1900, orbits 1 and 2; ×, O I] λ1356, orbit 3; □, O I] λ1356, orbits 4 to 6.) Vertical error bars are uncertainties in tilts; horizontal bars are the ranges of jovian magnetic latitudes through which Io passed during the orbit. The solid line is the tilt of the local jovian magnetic field (calculated from an offset tilted dipole model with no plasma currents) with respect to Io's south pole, in the plane containing Io and Jupiter.

sure, and evidence for its presence on Io is slightly better (*38*). Alternatively, protons might travel along the magnetic field lines from Jupiter and be preferentially deposited near Io's poles, where the magnetic flux through the surface is greatest, aided perhaps by a thinner polar atmosphere or "funneling" by an intrinsic Ionian magnetic field. This H could be sputtered from the surface or dissociated from sublimated H_2S by the intense, field-aligned, energetic electron beams detected in Io's plasma wake by Galileo (*39*), or some other particle source; it could radiate by resonant scattering of solar H I Lyman-α or by recombination after ionization by the same particles.

Another possible source of this emission is simple reflection of the bright solar H I Lyman-α radiation from the surface of Io, which does not require iogenic H at all. This would require only a 5% geometric albedo at Io's poles; it is consistent with the lack of variation of the H I Lyman-α emission with time, and with the all-disk component of the emission (Fig. 6A). It is more difficult to explain the polar emission enhancement under this hypothesis. One possibility is that a patchy frost or other substance in Io's polar region has a higher albedo at 1216 Å than the equatorial surface. Io is known to have an unidentified surface component near its poles (*40*), but its albedo at 1216 Å is unknown and would have to be significantly different from that at higher wavelengths, where a polar enhancement is not seen (Fig. 6B). Another possibility is that SO_2, a strong absorber of H I Lyman-α [cross section $\sigma = 3.9 \times 10^{-17}$ cm^2 (*41*)], has a higher column density near Io's equator and therefore blocks reflection of H I Lyman-α in that region, making the poles appear bright by contrast. Io's SO_2 atmosphere is still poorly known, however. It may be azimuthally symmetric about the subsolar point (*42*); this would produce a ring of H I Lyman-α emission in our images, just within the limb. It may be patchy, with column densities large enough to block H I Lyman-α ($\sim 2.5 \times 10^{16}$ cm^{-2}) occurring only near active volcanic vents; this would produce a disk of H I Lyman-α emission with dark blotches in our images. This hypothesis also leaves unexplained the recent evidence of iogenic H II from the Galileo PWS (*43*) and PLS (*44*) experiments. Nonetheless, simple diffuse reflection probably contributes to, and might fully explain, the H I Lyman-α emission in our data.

Because either possibility—iogenic H or selective diffuse reflection from Io's poles—has important consequences for our understanding of Io's surface and atmosphere, it is important to determine the extent to which each is responsible for Io's H I Lyman-α emission, and in particular for the polar patches. Possible STIS observations that

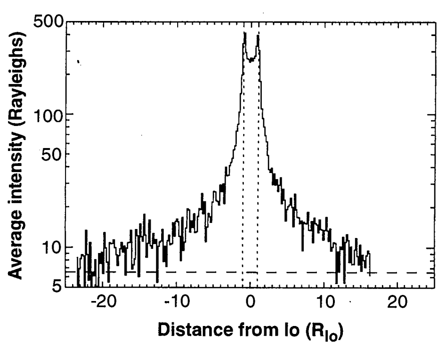

Fig. 4. Spatial profile of S I λ1479 emission from orbits 4 to 6. The six images were combined and binned 4 by 4 to reduce noise; they were then averaged across the combined slit widths of the S I λ1479 multiplet and are plotted here along the slit length. The horizontal dashed line marks the average background, as determined from the shadow of the slit's fiducial bar (the dip at $\sim -21\ R_{Io}$); the vertical dotted lines mark Io's position. Plots of the other S and O lines are similar.

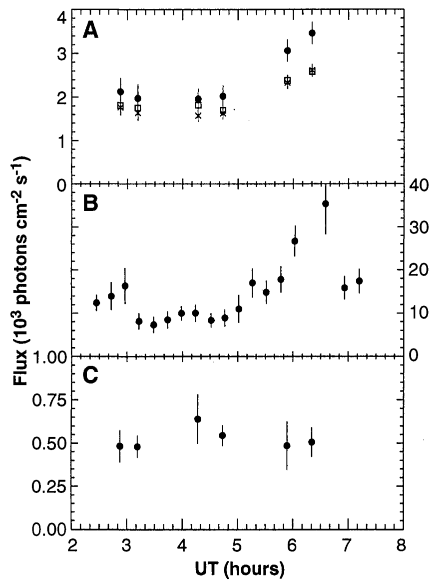

Fig. 5. H I, O I, and S I iogenic emission fluxes versus time for orbits 4 to 6 (14 October 1997). (**A**) S I λ1479 (●), O I] λ1356 (×), and O I λ1304 and S I λ1299 combined (□) STIS fluxes integrated over 2 arc sec by 4 arc sec boxes centered on Io at the appropriate wavelengths. (**B**) [O I] λ6300 fluxes from ground-based spectra acquired through a 5.2 arc sec by 5.2 arc sec squared aperture centered on Io. (**C**) H I Lyman-α STIS fluxes integrated over small boxes enclosing the emission features only (to reduce airglow contamination).

Table 3. Fluxes of O and S multiplets observed during orbits 4 to 6 (14 October), integrated over a 2 arc sec by 4 arc sec box centered on Io (*34*).

Species	Wavelength (Å)	Flux (10^{-3} photons cm^{-2} s^{-1})		
		Orbit 4	Orbit 5	Orbit 6
H I	1216	0.48 ± 0.06*	0.59 ± 0.08*	0.50 ± 0.08*
		0.41 ± 0.07†	0.64 ± 0.09†	0.32 ± 0.09†
O I + S I	1300	1.78 ± 0.11	1.75 ± 0.09	2.49 ± 0.09
O I	1356	1.70 ± 0.13	1.60 ± 0.10	2.48 ± 0.10
S I	1389	1.13 ± 0.15	1.27 ± 0.11	1.91 ± 0.11
	1429	0.88 ± 0.17	1.03 ± 0.14	1.44 ± 0.14
	1479	2.04 ± 0.22	1.99 ± 0.17	3.26 ± 0.17

*H I fluxes are from the two bright polar patches, with an off-Io background subtracted by the average of three different methods: subtraction of a simple average of boxes directly above and below the emission, subtraction of a linear fit to the background emission, and smoothing of the image followed by subtraction of a linear background fit. The three methods gave comparable results. †H I fluxes are from the two bright polar patches, subtracting a background found by averaging an equatorial band $0.5 R_{Io}$ wide on Io (Fig. 6).

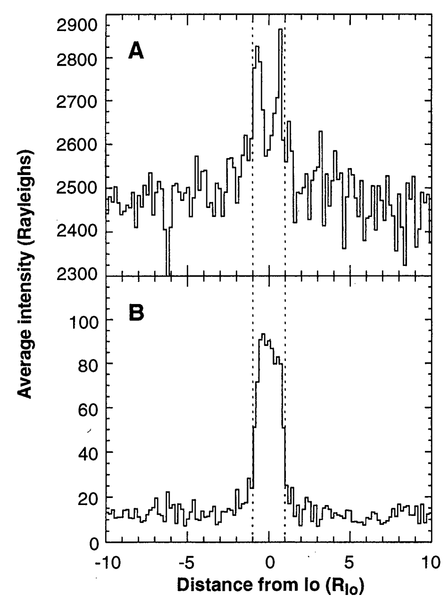

Fig. 6. (**A**) Spatial profile of H I Lyman-α emission from orbits 4 to 6. To reduce airglow noise, we used only the second image from each orbit. The three images were combined, binned 4 by 4, and averaged across a reduced slit width of 1.37 arc sec (1.25 R_{Io}), centered on Io at 1215.6 Å. The vertical dotted lines mark the edges of Io's disk. In addition to the two sharp peaks, corresponding to the patches seen in Figs. 1 and 2, there is an intensity enhancement over the entire disk. The dip at $\sim -6\ R_{Io}$ is the shadow of the far-UV MAMA repeller wire. (**B**) Spatial profile of reflected solar continuum from orbits 4 to 6. The six images were combined, binned 4 by 4, and averaged over 1512 to 1642 Å, a spectral range free of known emission lines.

would help make this determination are observations over a greater range of magnetic latitudes, to look for changes suggesting a connection with magnetospheric processes; at both east and west elongations, to see if the patches are fixed on Io's surface; during eclipse, to verify that solar H I Lyman-α (whether by diffuse reflection or resonant scattering) is responsible for the emission; and at high spectral resolution, to determine whether the emission from Io has the distinctive solar lineshape and to separate the Ionian emission from terrestrial airglow with a suitable velocity difference.

References and Notes

1. F. Scherb and W. H. Smyth, *J. Geophys. Res.* **98**, 18729 (1993).
2. J. T. Trauger, K. R. Stapelfeldt, G. E. Ballester, J. T. Clarke, WFPC2 Science Team, *Bull. Am. Astron. Soc.* **29**, 1002 (1997).
3. G. E. Ballester *et al.*, *Astrophys. J.* **319**, L33 (1987).
4. G. E. Ballester *et al.*, *Bull. Am. Astron. Soc.* **29**, 980 (1997).
5. J. T. Clarke, J. Ajello, J. Luhmann, N. M. Schneider, I. Kanik, *J. Geophys. Res.* **99**, 8387 (1994).
6. S. T. Durrance *et al.*, *Astrophys. J.* **447**, 408 (1995).
7. G. K. Fox *et al.*, *Astronom. J.* **113**, 1158 (1997); B. R. Sandel and A. L. Broadfoot, *J. Geophys. Res.* **87**, 212 (1982); J. R. Spencer and N. M. Schneider, *Annu. Rev. Earth Planet. Sci.* **24**, 125 (1996).
8. B. E. Woodgate *et al.*, *Proc. Astron. Soc. Pacific* **110**, 1183 (October 1998).
9. R. A. Kimble *et al.*, *Astrophys. J.* **492**, L83 (1998).
10. In time-tag mode, each photon's arrival time and position in the STIS multi-anode microchannel array (MAMA) are recorded individually.
11. M. Voit, Ed., *HST Data Handbook* (Space Telescope Science Institute, Baltimore, ed. 3.0, 1997).
12. The slit was effectively reduced to 30 arc sec by 2 arc sec (September) and 25 arc sec by 2 arc sec (October) by the finite size of the MAMA detectors.
13. The STIS is equipped with two MAMAs, which have different photocathodes sensitive to different wavelength ranges (*8*). Unfortunately, the NUV MAMA (covering 1650 to 3100 Å) was found after launch to have a dark rate exceeding design specification by about an order of magnitude, as a result of excessive phosphoresence in its MgF_2 window (*9*). Consequently, our G230M data (orbits 1 and 2) are noisy, and only the brightest features can be distinguished; these data are largely excluded from this paper.
14. It is unclear whether the near-Io emission at $\sim$1250 Å is predominately S I λ1251 or S II λ1256.
15. A. S. McEwen *et al.*, *Geophys. Res. Lett.* **24**, 2443 (1997).
16. T. E. Smith, M. A. McGrath, P. Sartoretti, *Bull. Am. Astron. Soc.* **27**, 1157 (1995).
17. G. E. Ballester *et al.*, in *Magnetospheres of the Outer Planets* (Boulder, CO, March 1997), unpublished proceedings.
18. One Rayleigh is 10^6 photons 4π sr^{-1} cm^{-2} s^{-1}.
19. Io's electrodynamic interaction with the plasma torus is typical of plasma flowing past an obstacle. In this case it is sub-Alfvénic ($v_{plasma} \sim 57$ km/s, $v_A \sim 300$ km/s), with no bowshock forming and standing magnetohydrodynamic Alfvén waves in Io's rest frame. The corotational electric field of 0.114 V/m produces a $\sim$400-kV voltage drop across Io, driving a current of a few million amperes through Io's ionosphere; Alfvén waves carry the current along the essentially equipotential magnetic field lines into Io's inner hemisphere and away from its outer hemisphere. (Electrons, the likely current carriers, would of course flow in the opposite direction.) The current loop can be completed in Jupiter's ionosphere only if the round trip travel time for an Alfvén wave is short compared with the time it takes for torus plasma to sweep past Io; otherwise, the current loop is closed in the plasma torus (*45*).
20. J. Saur, F. M. Neubauer, D. F. Strobel, M. E. Summers, in preparation.
21. M. G. Kivelson *et al.*, *Science*, **273**, 337 (1996); M. G. Kivelson *et al.*, *ibid.* **274**, 396 (1996).
22. P. E. Geissler *et al.*, *Bull. Am. Astron. Soc.* **30**, 1116 (1998).
23. A. S. McEwen *et al.*, *Icarus* **135**, 181 (1998).
24. Jupiter's magnetic equator is tilted 9.6° with respect to its spin equator and Io's orbital plane. Jupiter's centrifugal equator—the locus of points that, of all points on a magnetic field line, are the farthest from Jupiter's spin axis—lies between the magnetic and spin equators. The Io plasma torus is densest at, and approximately symmetric about, the centrifugal equator.
25. R. C. Woodward Jr. and W. H. Smyth, *Bull. Am. Astron. Soc.* **26**, 1139 (1994).
26. L. A. Frank *et al.*, *Science* **274**, 394 (1996).
27. F. Bagenal *et al.*, *Geophys. Res. Lett.* **24**, 2119 (1997).
28. R. J. Oliversen *et al.*, *Bull. Am. Astron. Soc.* **29**, 1315 (1997).
29. F. Scherb, K. D. Retherford, R. C. Woodward Jr., W. H. Smyth, *ibid.* **28**, 1155 (1996).
30. D. L. Judge and R. W. Carlson, *Science* **183**, 317 (1974).
31. F. M. Wu, P. Gangopadhyay, D. L. Judge, *J. Geophys. Res.* **100**, 3481 (1995).
32. The terrestrial glow still contributed significant photon noise to our data, especially because we made these observations 2 months after opposition, and a fraction of the Earth's exosphere along our line of sight was therefore sunlit. This effect was most pronounced at the beginning of each orbit.
33. E. Lellouch, *Icarus* **124**, 1 (1996).
34. No correction has been made for the fact that Io blocks part of the H I Lyman-α emission from the interplanetary medium; all Io H I Lyman-α intensities given in this research article could therefore be 200 to 900 Rayleighs too low. Fluxes given in row 2 of Table 3 are not subject to this correction.
35. D. B. Nash and R. R. Howell, *Science* **244**, 454 (1989).
36. A. S. McEwen, T. V. Johnson, D. L. Matson, L. A. Soderblom, *Icarus* **75**, 450 (1988).
37. E. Lellouch *et al.*, *ibid.* **98**, 271 (1992).
38. F. Salama *et al.*, *ibid.* **107**, 413 (1994); R. W. Carlson *et al.*, *Geophys. Res. Lett.* **24**, 2479 (1997).
39. D. J. Williams *et al.*, *Science* **274**, 401 (1996).
40. J. R. Spencer and N. M. Schneider, *Annu. Rev. Earth Planet. Sci.* **24**, 125 (1996).
41. S. A. Manatt and A. L. Lane, *J. Quant. Spectrosc. Radiat. Transfer* **50**, 267 (1993).
42. M. C. Wong and R. E. Johnson, *J. Geophys. Res.* **101**, 23243 (1996).
43. T. Chust, A. Roux, S. Perraut, D. A. Gurnett, *Ann. Geophys.* **15**, C824 (1997).
44. L. A. Frank, W. R. Paterson, K. L. Ackerson, S. J. Bolton, *Eos* **79**, S201 (1998).
45. D. A. Wolf-Gladrow, F. M. Neubaer, M. Lussem, *J. Geophys. Res.* **92**, 9949 (1987).

46. We thank D. Hall for valuable assistance in planning this experiment, and J. Corliss and M. Freed for long hours spent in data reduction. We also gratefully acknowledge the cooperation and assistance of our co-workers on the STIS Instrument Development Team, and the many people at the Space Telescope Science Institute whose work made these observations possible. We thank anonymous reviewers for valuable comments on the manuscript. A portion of D.F.S.'s research was accomplished at the Observatoire de Paris-Meudon; he thanks Département de Recherche Spatiale for its hospitality. This work was supported by NASA grants NAGW-3319, NAG-4168, and NAGW-6546, and NASA contracts NAS5-30131 and NAS5-30403.

24 August 1998; accepted 10 December 1998

Fusion-Competent Vaccines: Broad Neutralization of Primary Isolates of HIV

Rachel A. LaCasse, Kathryn E. Follis, Meg Trahey, John D. Scarborough,* Dan R. Littman, Jack H. Nunberg†

Current recombinant human immunodeficiency virus (HIV) gp120 protein vaccine candidates are unable to elicit antibodies capable of neutralizing infectivity of primary isolates from patients. Here, "fusion-competent" HIV vaccine immunogens were generated that capture the transient envelope-CD4-coreceptor structures that arise during HIV binding and fusion. In a transgenic mouse immunization model, these formaldehyde-fixed whole-cell vaccines elicited antibodies capable of neutralizing infectivity of 23 of 24 primary HIV isolates from diverse geographic locations and genetic clades A to E. Development of these fusion-dependent immunogens may lead to a broadly effective HIV vaccine.

The expanding epidemic of HIV infection threatens to engulf more than 40 million persons worldwide by the year 2000 (*1*). The need for an effective HIV vaccine is urgent, but progress toward this goal has been slowed in part by the inability of any vaccine candidate to elicit antibodies capable of neutralizing infectivity of primary HIV isolates (PIs) from infected individuals (*2, 3*).

Because the HIV envelope protein mediates the early binding and entry steps in infection, many vaccine strategies have focused on this target. In 1993, two recombinant forms of the surface gp120 subunit of the HIV envelope protein (rgp120) were advanced as candidate vaccines for a large-scale efficacy study sponsored by the National Institutes of Health

R. A. LaCasse, K. E. Follis, M. Trahey, J. H. Nunberg, The Montana Biotechnology Center and Division of Biological Sciences, University of Montana, Missoula, MT 59812, USA. J. D. Scarborough and D. R. Littman, Howard Hughes Medical Institute, Skirball Institute of Biomolecular Medicine, New York University Medical Center, 540 First Avenue, New York, NY 10016, USA.

*Present address: Oregon Health Sciences University, Portland, OR 97201, USA.

†To whom correspondence should be addressed. E-mail: nunberg@selway.umt.edu